Synthesis of $ZnFe_2O_4$ nanomagnets by Fe-ion implantation into ZnO and post-annealing*

Pan Feng(潘 峰)[a)b)], Guo Ying(郭 颖)[b)], Cheng Feng-Feng(成枫锋)[a)], Fa Tao(法 涛)[a)], and Yao Shu-De(姚淑德)[a)†]

[a)] *State Key Laboratory of Nuclear Physics and Technology, Peking University, Beijing* 100871, *China*

[b)] *Department of Physics, Shaanxi University of Technology, Hanzhong* 723001, *China*

(Received 10 July 2011; revised manuscript received 28 July 2011)

Fe ions of dose 8×10^{16} cm^{-2} are implanted into a ZnO single crystal at 180 keV. Annealing at 1073 K leads to the formation of zinc ferrite ($ZnFe_2O_4$), which is verified by synchrotron radiation X-ray diffraction (SR-XRD) and X-ray photoelectron spectroscopy (XPS). The crystallographically oriented $ZnFe_2O_4$ is formed inside the ZnO with the orientation relationship of $ZnFe_2O_4$ (111)//ZnO (0001). Superconducting quantum interference device (SQUID) measurements show that the as-implanted and post-annealing samples are both ferromagnetic at 5 K. The synthesized $ZnFe_2O_4$ is superparamagnetic, with a blocking temperature (T_B = 25 K), indicated by zero field cooling and field cooling (ZFC/FC) measurements.

Keywords: Fe implanted, ZnO, $ZnFe_2O_4$, superparamagnetic

PACS: 75.50.Pp, 61.72.uj, 61.46.Df, 75.60.Ej **DOI:** 10.1088/1674-1056/20/12/127501

1. Introduction

Diluted magnetic semiconductors (DMSs) are expected to play an important role in spintronic applications such as the injection of spin polarized currents. In particlular, ZnO-based DMS has attracted extensive attention due to the the fact that Dietl *et al.*[1] predicted that ferromagnetism at above room temperature could be obtained. In the last decade, a large number of research groups reported on the ferromagnetism in ZnO-doped transition metals (TMs) (from Sc to Ni) fabricated by various methods.[2−7] In contrast to these results, other groups reported on the observations of antiferromagnetism,[8] spin-glass behaviour,[9] and paramagnetism[10,11] in TM-doped ZnO. Moreover, superparamagnetic Fe, Co, and Ni nanoclusters were formed by ion implantation into ZnO,[12−15] separately. Therefore, the origin for the reported ferromagnetism in ZnO-based DMS remains very questionable. One of the main obstacles in creating DMS materials is the formation of secondary phase because of the solid-solubility limit of magnetic ions in semiconductor hosts. The synchrotron radiation X-ray diffraction (SR-XRD) is a powerful tool to detect small precipitates, e.g., metallic TM nanocrystals and secondary phase in TM-implanted ZnO.[16,17] In this paper, employing the SR-XRD, X-ray photoelectron spectroscopy (XPS) and superconducting quantum interference device (SQUID), we study the structure, the chemical bonding state, and the magnetic property of Fe-implanted ZnO. Moreover, the possibility to form superparamagnetic $ZnFe_2O_4$ nanocrystals embedded in ZnO is demonstrated.

2. Experiment

Commerical ZnO bulk crystal was implanted with ^{57}Fe ions at an energy of 180 keV, with a fluence of 8×10^{16} cm^{-2} at room temperature. The injected range was calculated using the TRIM code (Fig. 1), showing that the implantation depth at the maximum density is R_p = 81 nm, with straggling ΔR_p = ±35 nm. After being analysed, the as-implanted samples were annealed at 1073 K for 30 min under vacuum.

Structural analysis was performed by SR-XRD at the National Synchrotron Radiation Laboratory

*Project supported by the National Basic Research Program of China (Grant No. 2010CB832904), the National Natural Science Foundation of China (Grant Nos. 10875007 and 11005005), and the Research Fund of Shaanxi University of Technology, China (Grant No. SLQ0815).

†Corresponding author. E-mail: sdyao@pku.edu.cn

© 2011 Chinese Physical Society and IOP Publishing Ltd

(NSRL, Hefei, China) with an X-ray wavelength of 0.153981 nm. θ–2θ scans were used to identify crystalline precipitates. The chemical bonding states were analysed by Kratos Axis Ultra X-ray photoelectron spectroscopy with monochromatized Al Kα radiation (1486.8 eV) and Cls (E = 284.8 eV) level serving as the internal standard. The magnetic properties were measured with a SQUID magnetometer (Quantum Design MPMS) in a temperature range of 5 K–350 K, which is capable of detecting a magnetic moment as small as 10^{-8} emu. By magnetic measurement, virgin ZnO was found to be purely diamagnetic, with a susceptibility of -2.65×10^{-7} emu/Oe·g (1 Oe=79.5775 A/m). This background was subtracted from the magnetization data. To measure the temperature-dependent magnetization separately, after zero field cooling (ZFC) and field cooling (FC), the samples were cooled in zero field from above room temperature to 5 K. Then a 50-Oe field was applied. The ZFC curve was measured with temperature increasing from 5 K to 350 K, after which the FC curve was measured in the same field with temperature decreasing from 350 K to 5 K.

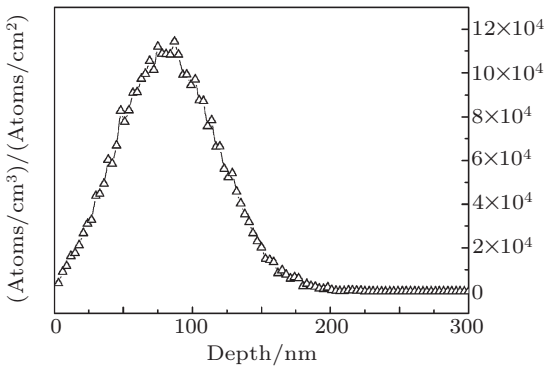


Fig. 1. Depth profile of Fe in ZnO, calculated by TRIM code.

3. Results and discussion

Figure 2 show the SR-XRD patterns for the as-implanted and annealed samples. For the as-implanted samples, crystalline α-Fe was observed, and no other crystalline Fe-oxide (Fe_2O_3, Fe_3O_4, and $ZnFe_2O_4$) particles were detected. After 30-min annealing at 1073 K, the Fe (110) peak almost disappeared and the sample already shows three peaks of $ZnFe_2O_4$ (222), (333), and (444), which means that the crystallites of $ZnFe_2O_4$ are highly oriented with respect to the host matrix. The inset shows the XRD ω-rocking curve of $ZnFe_2O_4$ (333) peak, demonstrating the single crystal quality of the nanocrystal with a full width at half maximum (FWHM) of 0.963°. Since XRD peak positions of Fe_3O_4 and $ZnFe_2O_4$ match closely, it is difficult to identify the phase using XRD pattern only. We will discuss this further while analyzing XPS data. The average crystallite size of $ZnFe_2O_4$ (8 nm) was calculated using the Scherrer formula,[18]

$$d = 0.9\lambda/(\beta \cos\theta), \tag{1}$$

where λ is the wavelength of the X-ray, θ is the Bragg angle, and β is the FWHM of 2θ in radians. The parameter of $ZnFe_2O_4$ is found to be 0.8439 nm, slightly smaller than the 0.8443 nm value reported for bulk zinc ferrite (PCPDF No. 89-4926). When the particle size decreases to the nanometer-sized scale, the surface area greatly increases, which enhances the energy of the system, making these nanometer-sized $ZnFe_2O_4$ particles contracted in the lattice. This is consistent with the other observation.[19]

Note the symmetry of the ZnO (0002) and (0004) diffraction peaks of the as-implanted sample in Fig. 2. Shoulders on the right side (smaller lattice constant) are clearly observed. These shoulders can be related to lattice damage or ZnO substituted with Fe. In view of a detailed study of Co ion implantation into ZnO,[20] the shoulder (on the right side) is interpreted in terms of ternary $Zn_{1-x}Co_xO$, formed due to the incorporation of Co into the Zn sublattice of the ZnO host crystal. We rather attribute the observed right-side shoulders to Zn substituted with Fe. After 30-min annealing at 1073 K, zinc ferrite started to form, therefore these shoulders disappeared.

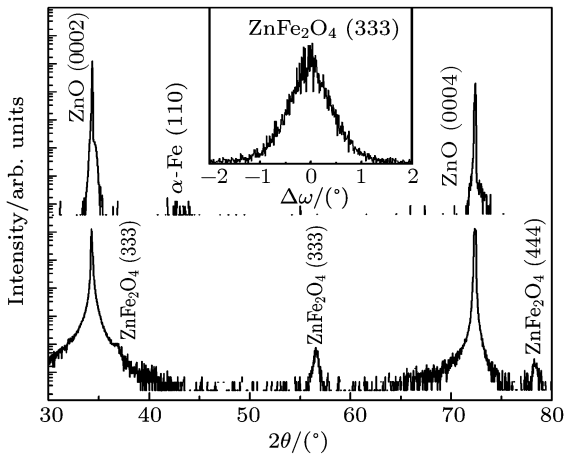


Fig. 2. SR-XRD patterns for the as-implanted (up) and annealed at 1073 K (down) samples. The inset shows the ω-rocking curve of $ZnFe_2O_4$(333) peak.

Figure 3(a) shows typical results of the ϕ-scans for the sample annealed at 1073 K, revealing the crystallographical orientation relationship between $ZnFe_2O_4$

and the ZnO matrix. The azimuthal coordinate (ϕ) is the angle of rotation about the surface normal. As a standard approach, for an XRD ϕ-scan one first tilts the sample by the angle χ from the sample surface and fixes the Bragg angle θ. Subsequently the spectrum is recorded during azimuthal rotation with respect to the sample normal. χ can be calculated by the the following equations: for cubic structure,

$$\cos\chi = \frac{h_1h_2 + k_1k_2 + l_1l_2}{\sqrt{(h_1^2 + k_1^2 + l_1^2)\,(h_2^2 + k_2^2 + l_2^2)}}; \qquad (2)$$

for hexagonal structure,

$$\cos\chi = \frac{h_1h_2 + k_1k_2 + (h_1k_2 + h_2k_1)/2 + 3a^2l_1l_2/(4c^2)}{\sqrt{(h_1^2 + k_1^2 + h_1k_1 + 3a^2l_1^2/(4c^2))\,(h_2^2 + k_2^2 + h_2k_2 + 3a^2l_2^2/(4c^2))}}, \qquad (3)$$

where χ is the angle between the diffraction plane of interest ($h_2k_2l_2$) and the sample surface ($h_1k_1l_1$). As expected from the crystalline symmetry, the ZnO (0001) and $ZnFe_2O_4$(111) show six-fold symmetry at the same azimuthal position (note that the measurements were only performed with ϕ ranging from 0° to 180°). Therefore, we can conclude that $ZnFe_2O_4$ is crystallographically oriented with respect to the ZnO matrix. From all the above diffraction data, the surface orientation relations between the ZnO and the $ZnFe_2O_4$ are $ZnFe_2O_4$ (111)//ZnO (0001). Due to the hexagonal structure of six-fold symmetry of $ZnFe_2O_4$ viewed along the [111] direction, it is not difficult to understand their crystallographical orientation onto hexagonal ZnO.

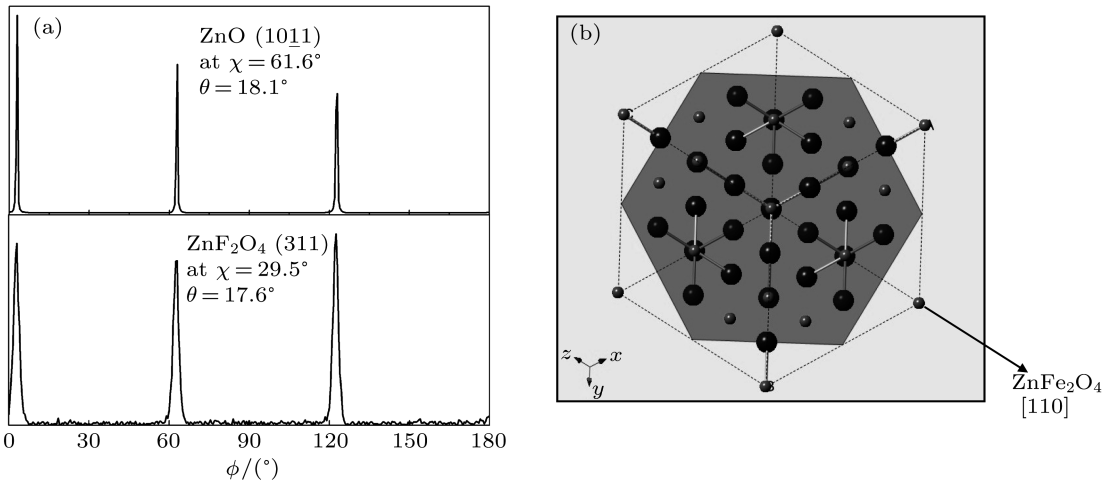


Fig. 3. (a) SR-XRD ϕ-scans of ZnO (10$\bar{1}$1) and $ZnFe_2O_4$ (311) for the sample annealed at 1073 K, revealing the in-plane orientation relationship for $ZnFe_2O_4$ with respect to ZnO. (b) $ZnFe_2O_4$ (111) showing six-fold symmetry viewed along the [111] direction.

Since the crystal structures of Fe_3O_4 and $ZnFe_2O_4$ are quite similar (their lattice parameters are 0.8395 nm and 0.8433 nm, respectively), the possibility of the presence of Fe_3O_4 (magnetite) cannot be ruled out only by the X-ray diffraction patterns. To confirm the phases of $ZnFe_2O_4$ presented in the sample, the X-ray photoelectron spectroscopy was performed to analyse the chemical bonding states of elements. In $ZnFe_2O_4$, Fe and Zn atoms exist in the lattice with more than one chemical state (A-sites or B-sites), bringing about several different contributions with different binding energies in the X-ray photoelectron spectroscopy spectra. Figure 4(a) shows the detailed analysis of the Zn $2p_{3/2}$ peak: experiment date (square) and the fitting using two Gaussian functions for decomposition into two major peaks at 1021.8 eV and 1021.5 eV with widths 1.2 eV and 2.2 eV respectively. Bear *et al.*[21] have found the Zn $2p_{3/2}$ comes from two parts in mixture of ZnO and $ZnFe_2O_4$. Druska *et al.*[22] have reported that the binding energy of Zn $2p_{3/2}$ is around 1023.0 eV in $ZnTiO_3$ where zinc occupies the octahedral sites. The peak at 1021.5 eV is consistent with the X-ray photoelectron spectroscopy recorded for the standard $ZnFe_2O_4$ materials.[23] Hence we assume that the peak at 1021.5 eV is ascribed to the formation of zinc ferrite with the zinc atom occupying only tetrahedral sites. The other peak at 1021.8 eV should be due to ZnO.

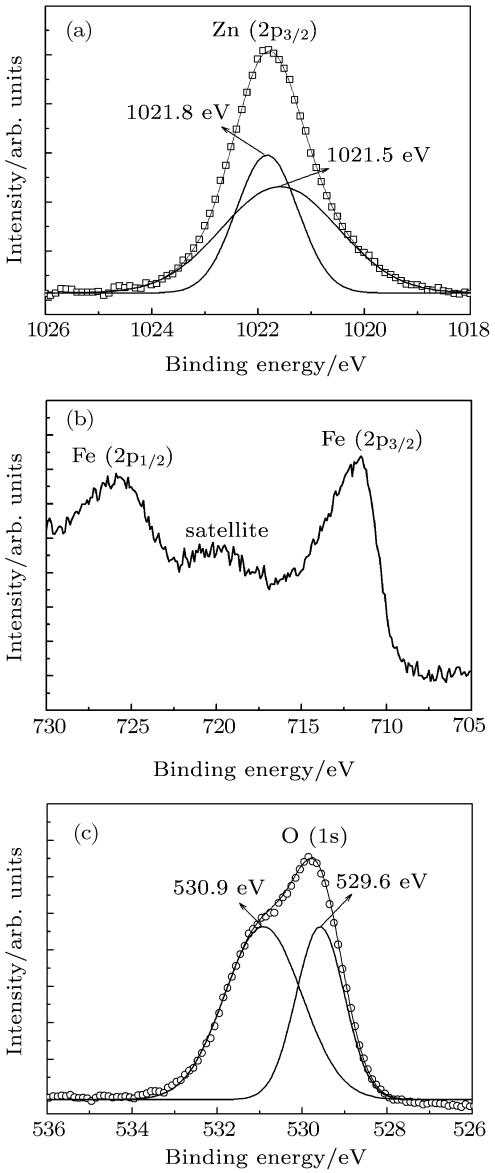


Fig. 4. X-ray photoelectron spectra for the samples annealed at 1073 K: (a) Zn 2p, (b) Fe 2p, (c) O 1s.

The Fe $2p_{3/2}$ photoelectron peak is always related to the background, which makes the analysis of the peak complicated. Due to spin–orbit coupling, the Fe 2p core level splits into $2p_{1/2}$ and $2p_{3/2}$ components. Figure 4(b) shows the Fe 2p peaks at binding energies of 725.6 eV and 711.5 eV, with a shakeup satellite at 719.0 eV. The binding energy for Fe $2p_{3/2}$ in $ZnFe_2O_4$ is 711.5 eV, which matches well with the value reported in Ref. [21]. In magnetite (Fe_3O_4), the Fe $2p_{3/2}$ peak is contributed from $2Fe^{3+}$ and $1Fe^{2+}$ ions. The Fe $2p_{3/2}$ binding energy values for Fe^{2+} and Fe^{3+} are 709.2 eV and 711.1 eV, respectively.[24] Fe^{3+} is the dominant species in magnetite, and the peak centre was observed at the higher binding energy side, i.e., at 710.6 eV in comparison to the Fe^{2+} binding energy at 709.5 eV.[24] In the case of zinc ferrite, the system does not contain any Fe^{2+}, so the binding energy increases to 711.5 eV in comparison to Fe_3O_4. In Fe_3O_4, the satellite peak associated with $2p_{3/2}$ of Fe is not seen or it may be absent because of the superposition of the satellites.[25] The XPS analysis confirms that the $ZnFe_2O_4$ is formed in the post-annealed sample.

The O 1s XPS spectrum shows a broad asymmetric curve which is fitted by two peaks, with binding energies at 530.9 eV and 529.6 eV in Fig. 4(c). The peak at 529.6 eV is characteristic of oxygen in the (Zn/Fe)-oxygen framework, and the other peak at around 530.9 eV is ascribed to the oxygen in the adsorbed OH^- groups on the sample surface.[26,27]

The bulk zinc ferrite belongs to the normal spinel type and behaves paramagnetically at room temperature.[28] However, recent experiments revealed that Zn ferrite in the nanometric range presents ferromagnetic behaviour below a blocking temperature (T_B).[29–31] Figures 5(a) and 5(b) show the variations of magnetization with applied field at 5 K. Magnetic hysteretic loops are observed for the as-implanted sample and the annealed sample at 1073 K, and attributed to α–Fe and $ZnFe_2O_4$ nanoparticles, respectively.

In order to confirm the superparamagnetic property of the embedded $ZnFe_2O_4$ nanoparticles, the measurements of ZFC/FC magnetization versus temperature were performed using SQUID. Figure 5(c) shows the temperature dependences of magnetization by the ZFC and FC procedures from 5 K to 350 K in an applied magnetic field of 50 Oe. The ZFC curve shows a gradual increase at low temperatures, and reaches a plateau at a particular temperature of T_B, while the FC curve continues to increase with decreasing temperature. In this paper, the temperature (T_B) at the maximum of the ZFC curve is taken as the average blocking temperature. The shapes of the ZFC/FC curves are the typical characteristics for magnetic nanoparticle systems with a broad size distribution.[32,33] The broad peak in the ZFC curve is due to the size distribution of $ZnFe_2O_4$ nanocrystals. The discrepancy between the ZFC and the FC curve at a lower magnetic field demonstrates that $ZnFe_2O_4$ nanocrystals are superparamagnetic, with an apparent blocking temperature ($T_B = 25$ K). Below this temperature, an expected ferromagnetic response becomes evident as reflected in Fig. 5(b) for M–H measurements at $T < 25$ K.

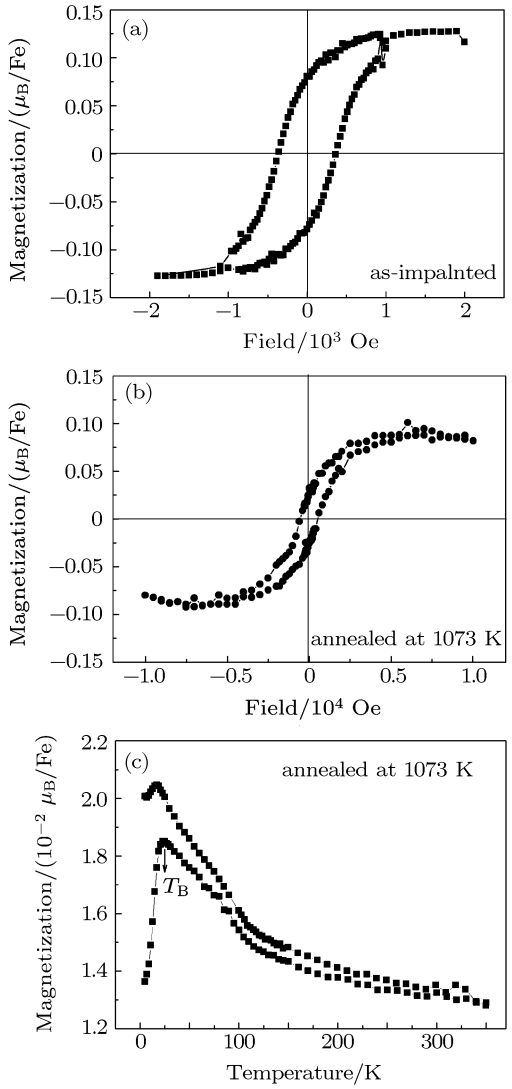


Fig. 5. *M–H* curves of the sample at 5 K: (a) as-implanted and (b) annealed at 1073 K. (c) ZFC and FC magnetization curves at 50 Oe for the annealed sample, which exhibit a typical characteristic of a magnetic nanoparticle system.

4. Conclusion

In this paper, we studied the formation of secondary phase in Fe-implanted ZnO by SR-XRD, XPS, and SQUID. In the as-implanted sample, α–Fe is the origin of the ferromagnetism, while 1073-K post-annealing induces the growth of superparamagnetic $ZnFe_2O_4$ nanocrystals. The crystallographically oriented $ZnFe_2O_4$ nanocrystals are formed inside ZnO with the orientation relationship of $ZnFe_2O_4$ (111) // ZnO (0001). Thus, a hybrid structure of spinel ferrites/semiconducting ZnO could be a potential candidate for spintronic devices.

References

[1] Dietl T, Ohno H, Matsukura F, Cibert J and Ferrand D 2000 *Science* **287** 1019

[2] Liu S H, Hsu H S, Venkataiah G, Qi X, Lin C R, Lee J F, Liang K S and Huang J C A 2010 *Appl. Phys. Lett.* **96** 262504

[3] Lu Z L, Zou W Q, Xu M X and Zhang F M 2010 *Chin. Phys.* B **19** 056101

[4] Cheng X W, Li X, Gao Y L, Yu Z, Long X and Liu Y 2009 *Acta Phys. Sin.* **58** 2018 (in Chinese)

[5] Wang D, Chen Z Q, Zhou F, Lu W, Maekawa M and Kawasuso A 2009 *Appl. Surf. Sci.* **255** 9371

[6] Li M, Zou C W, Wang G F, Wang H J, Yin M L, Liu C S, Guo L P, Fu D J and Kang T W 2010 *J. Appl. Phys.* **107** 104117

[7] Liu X J, Zhu X Y, Song C, Zeng F and Pan F 2009 *J. Phys.* D: *Appl. Phys.* **42** 035004

[8] Yin S, Xu M X, Yang L, Liu J F, Rösner H, Hahn H, Gleiter H, Schild D, Doyle S, Liu T, Hu T D, Takayama-Muromachi E and Jiang J Z 2006 *Phys. Rev.* B **73** 224408

[9] Jin Z W, Fukumura T, Kawasaki M, Ando K, Saito H, Sekiguchi T, Yoo Y Z, Murakami M, Matsumoto Y, Hasegawa T and Koinuma H 2001 *Appl. Phys. Lett.* **78** 3824

[10] Liu X C, Shi E W, Song L X, Zhang H W and Chen Z Z 2006 *Acta Phys. Sin.* **55** 2557 (in Chinese)

[11] Xu Q Y, Zheng X H and Gong Y P 2010 *Chin. Phys.* B **19** 077501

[12] Zhou S, Potzger K, Talut G, Reuther H, von Borany J, Grötzschel R, Skorupa W, Helm M, Fassbender J, Volbers N, Lorenz M and Herrmannsdörfer T 2008 *J. Appl. Phys.* **103** 023902

[13] Norton D P, Overberg M E, Pearton S J, Pruessner K, Budai J D, Boatner L A, Chisholm M F, Lee J S, Khim Z G, Park Y D and Wilson R G 2003 *Appl. Phys. Lett.* **83** 5488

[14] Zhou S, Potzger K, Zhang G F, Eichhorn F, Skorupa W, Helm M and Fassbender J 2006 *J. Appl. Phys.* **100** 114304

[15] Zhou S, Potzger K, von Borany J, Grötzschel R, Skorupa W, Helm M and Fassbender J 2008 *Phys. Rev.* B **77** 035209

[16] Zhou S, Potzger K, Talut G, von Borany J, Skorupa W, Helm M and Fassbender J 2008 *J. Appl. Phys.* **103** 07D530

[17] Zhou S , Potzger K, Xu Q Y, Talut G, Lorenz M, Skorupa W, Helm M, Fassbender J, Grundmann M and Schmidt H 2009 *Vacuum* **83** S13

[18] Cullity B D 1978 *Elements of X-ray Diffractions* (MA: Addison-Wesley Reading) pp. 102–103

[19] Yao C W, Zeng Q S, Goya G F, Torres T, Liu J F, Wu H P, Ge M Y, Zeng Y W, Wang Y W and Jiang J Z 2007 *J. Phys. Chem.* C **111** 12274

[20] Geurts J, Schumm M, Koerdel M, Ziereis C, Müller S, Ronning C, Dynowska E, Gołacki Z and Szuszkiewicz W 2010 *Phys. Status Solidi* B **247** 1469

[21] Bear S, Prince A A M, Velmurugan S, Raghavan P S, Gopalan R, Panneerselvam G and Narasimhan S V 2001 *J. Mater. Sci.* **36** 5379

[22] Druska P, Steinike U and Sepelak V 1999 *J. Solid State Chem.* **146** 13

[23] Tahir A A and Upul Wijayantha K G 2010 *J. Photochem. Photobio.* A: *Chem.* **216** 119

[24] Tiwari S, Prakash R, Choudhary R J and Phase D M 2007 *J. Phys.* D: *Appl. Phys.* **40** 4943

[25] Liu H, Jiang E Y, Zheng R K and Bai H L 2003 *J. Phys.: Condens. Matter* **15** 8003

[26] Marco J F, Gancedo J R, Gracia M, Gautier J L, Rios E and Berry F J 2000 *J. Solid State Chem.* **153** 74

[27] Tavares A C, da Silva Pereira M I, Mendonça M H, Nunes M R, Costa F M and Sá C M 1998 *J. Electroanal. Chem.* **449** 91

[28] Zhou Z H, Xue J M, Chan H S O and Wang J 2001 *J. Appl. Phys.* **90** 4169

[29] Bohra M, Prasad S, Kumar N, Misra D S, Sahoo S C, Venkataramani N and Krishnan R 2006 *Appl. Phys. Lett.* **88** 262506

[30] Shinagawa T, Izaki M, Inui H, Murase K and Awakura Y 2006 *Chem. Mater.* **18** 763

[31] Zhou S, Potzger K, Reuther H, Talut G, Eichhorn F, von Borany J, Skorupa W, Helm M and Fassbender J 2007 *J. Phys.* D: *Appl. Phys.* **40** 964

[32] Respaud M, Broto J M, Rakoto H, Fert A R, Thomas L, Barbara B, Verelst M, Snoeck E, Lecante P, Mosset A, Osuna J, Ould Ely T, Amiens C and Chaudret B 1998 *Phys. Rev.* B **57** 2925

[33] Tsoi G M, Wenger L E, Senaratne U, Tackett R J, Buc E C, Naik R, Vaishnava P P and Naik V 2005 *Phys. Rev.* B **72** 014445